NUMERICAL STUDY OF THE EFFECT OF EFFECTIVE DIFFUSIVITY AND PERMEABILITY OF THE GAS DIFFUSION LAYER ON FUEL CELL PERFORMANCE

Mamdud Hossain[1], Sheikh Zahidul Islam[1], Patricia Pollard[1]

[1]School of Engineering, Robert Gordon University, Schoolhill, Aberdeen, AB10 1FR, UK,

Corresponding Author:

Mamdud Hossain
School of Engineering, Robert Gordon University, Schoolhill, Aberdeen, AB10 1FR, UK,
Tel: +44(0)1224262351, Fax:+44(0)1224262444, Email: M.Hossain@rgu.ac.uk

ABSTRACT

A three-dimensional, single-phase, isothermal, explicit electro-chemistry polymer electrolyte membrane fuel cell model has been developed and the developed computational model has been used to compare various effective diffusivity models of the gas diffusion layer. The Bruggeman model has traditionally been used to represent the diffusion of species in the porous gas diffusion layer. In the present study, the Bruggeman model has been compared against models based on particle porous media, multi-length scale particles and the percolation type correlation. The effects of isotropic and anisotropic permeability on flow dynamics and fuel cell performance have also been investigated. The present study shows that the modelling of the effective diffusivity has significant effects on the fuel cell performance prediction. The percolation based anisotropic model provides better accuracy for the fuel cell performance prediction. The effects of permeability have been found to be negligible and the specification of any realistic value for permeability has been found to be sufficient for polymer electrolyte membrane fuel cell modelling.

Keywords: PEM fuel cell; anisotropy; effective diffusivity; permeability.

1 INTRODUCTION

Rapid growth of the economies in many countries of the world together with modern technological advancements in consumer goods has caused significant increase in the consumption of energy. Global energy demands are primarily met by combusting fossil fuels. Over reliance on fossil fuels to meet the growing energy demand already has major consequences in terms of climate change. Climate change is real and the emission of CO_2 has increased by a factor of three since the industrial revolution and is increasing at a faster rate [1]. Improved efficiency and energy savings will not be sufficient to meet future energy demand. In this regard, several alternative renewable energy sources such as wind turbine, solar photovoltaic, and hydrogen fuel cells have gained prominence to provide clean energy. Among these wind turbine technology has gained technical maturity and the wind energy installed capacity has reached 175 Gigawatt in 2010 [2]. The main disadvantage of wind and solar energy remains their intermittent availability and variation in energy density. In this regard, fuel cells are one of the clean sources of energy that can make a real contribution to the reduction of CO_2 emission. Among the many fuel cells such as direct methanol, solid oxide, molten carbonate, a polymer electrolyte membrane (PEM) fuel cell is the most versatile that can be used in residential and transport sectors.

Despite having many advantages, the wider deployment of polymer electrolyte membrane fuel cells has been hampered by high cost. The high cost of a polymer electrolyte membrane fuel cell results from using expensive Platinum in catalyst layers to initiate the electrochemical reaction. One of the methods for reducing the cost of a PEM fuel cell would be to develop new architecture that would produce more power per unit area of a PEM fuel cell. In this respect, a

computational model is an indispensible tool for developing and optimising a new fuel cell design provided the model is accurate. A fuel cell model needs to take into account complex electro-chemical reactions, diffusion of species, transport of electron, proton and transport of water. In order to handle these complex processes, often may simplified assumptions are made. In addition, many empirical correlations are used to treat physical processes. This often introduces many uncertainties in developing a computational tool. The focus of the present study is the accurate modelling of the transport of species through the gas diffusion layer (GDL) of a PEM fuel cell.

A gas diffusion layer is a critical component of a PEM fuel cell which provides both functional and structural support. The main function of a gas diffusion layer is to provide a passage for reactants from the flow channel to the catalyst layer and to remove produced water. It also carries electrons to facilitate electro-chemical reaction. The effective diffusivity of species through a gas diffusion layer has traditionally been modelled by the Bruggeman model. For example, some of the pioneering work in the development of three dimensional fuel cell models has implemented the Bruggeman model to account for the diffusion of species through the gas diffusion layer [3-7]. Pharoah et al [8] cited a comprehensive review of 100 papers on the modelling of PEM and direct methanol fuel cells and stated that species transport in the gas diffusion layer was modelled in all the papers by the Bruggeman correlation which was developed for a granular porous media. A gas diffusion layer is made of randomly distributed carbon fibres of 7-10 µm diameter and several millimetres long formed into paper or cloth, and clearly demonstrates anisotropic behaviour [8]. Nam and Kaviany [9] developed an effective diffusivity model on pore network modelling of a fibrous web. Their model was compared against a percolation based model of Tomadakis and Sotirchos [10] and a multi-length scale, particle

based porous media model of Mezedur et al [11]. Their study showed that the Tomadakis and Sotirchos [10] model better represented the effective diffusivity in a GDL as its takes into account the anisotropy of fibre distribution. Gostick et al. [12] experimentally studied the in-plane and through-plane permeability of several commercially available GDLs and showed that the in-plane permeability was much higher than the through-plane permeability. Gostick et al. [12] suggested that the Tomadakis and Sotirchos [10] model was also capable of accounting for the anisotropy in the diffusion coefficient by modelling the tortuosity more accurately.

The above literature review suggests that the Bruggeman correlation does not seem to represent the diffusivity of species through a GDL accurately. However, to the best of the authors' knowledge, there has not been any study that has systematically compared various effective diffusivity models for fuel cell performance prediction. Therefore, it is not clearly understood, how much of this uncertainty in modelling the effective diffusivity contributes to the actual modelling uncertainty of a PEM fuel cell. Sivertsen and Djilali [7] modified the Bruggeman model based on a constant tortuosity factor of 3 without providing justification for using such a value. Pharoah et al [8] treated the anisotropic gas transport inside a GDL by the percolation based anisotropic model of Tomadakis and Sotirchos [10] and showed that the anisotropic treatment had significant effects on the prediction of fuel cell voltage at current densities between 0.8-1.2 Acm^{-2}. Dawes et al [13] developed a percolation based isotropic diffusivity model. Their percolation based diffusivity model provided slightly better results compared to the Bruggeman model. Some recent work has focused on the anisotropic treatment of thermal conductivity of a GDL. In particular, Bapat and Thynell [14] investigated the effects of through-plane and in-plane thermal conductivity on the current density and the temperature distribution using a pseudo two-dimensional fuel cell geometry and concluded that an innovative GDL designed with a higher

through-plane thermal conductivity at the inlet and progressively decreasing through-plane thermal conductivity away from the inlet can lead to maximum potential. Ju [15] also investigated the effects of anisotropy in the thermal conductivity of a GDL on temperature distribution and water vapour characteristics and stated that the anisotropy had significant effects. In these studies, however, thermal conductivity values were not correlated with porosity, fibre orientations or GDL properties, instead, different ratios of through-plane and in-plane thermal conductivity were assumed. In the present study, a systematic comparison of various diffusivity models in predicting the performance of a PEM fuel cell has been reported.

The second objective of this study is to investigate the effects of permeability of a gas diffusion layer. A literature search of previous reported modelling studies shows that different values of permeability have been used. For example, an isotropic permeability value of 1.76×10^{-11} m^2 has been widely used [12, 16-18]. In addition, the permeability values of 10^{-12} m^2 [19-20] and 5×10^{-11} m^2 [13] have been used in the computational modelling studies of a PEM fuel cell. Dawes et al [13] gave an account of a parametric study of permeability values in the range of 1.5×10^{-8} to 1.5×10^{-12} m^2. Gostick et al [12] measured the through-plane and in-plane permeability of various commercially available gas diffusion layers to be in the range of 10^{-11} – 10^{-12} m^2. The effect of anisotropy in permeability was studied computationally by Ahmed et al. [21] by setting various combinations of in-plane and through plane permeabilities in the range of 1×10^{-9} to 1×10^{-15}. Their study showed that the permeability had significant effects on water and thermal management especially at very low values of permeability. In Ahmed et al.'s [21] study, the permeability values were arbitrarily set at unrealistically low values and the analysis was done for a single current density of 2.4 Acm^{-2}. This current density is unusually high. By contrast, Dawes et al [13] provided a parametric study of the effects of permeability on the cell

performance. They showed that the effect of permeability became insignificant below a permeability of 5×10^{-11}.

The literature review above clearly shows that there is uncertainty in modelling the effective diffusivity of species through a gas diffusion layer of a PEM fuel cell. Moreover, there is also uncertainty in the value of the permeability of a gas diffusion layer. The present study seeks to provide a systematic comparison of various effective diffusivity models and to investigate the effects of permeability of a gas diffusion layer on the PEM fuel cell performance.

2 NUMERICAL MODEL DEVELOPMENT

2.1 Modelling domain and Assumptions

In the present study, a representative straight channel has been utilized to demonstrate the effects of the effective diffusivity of reactants and products. Figure 1 shows a three-dimensional straight channel which consists of anode and cathode gas channels for transporting the reactants (oxygen and hydrogen) and the product (water vapour) mixed in air, to and from the porous gas diffusion layers. The electrochemical reactions occur at the catalyst layers and a polymer electrolyte membrane is sandwiched between the catalyst layers. Protons and water are transported through the membrane.

The assumptions used in the three-dimensional model are as follows:

- Steady-state operation,
- Isothermal operation,
- Ideal gas mixtures,

- All the porous zones in the fuel cell domain are assumed to be homogeneous, and the membrane is considered impervious to reactant gases,
- Water produced on the cathode side is in vapour phase.

2.2 Model equations

Governing Equations

The governing equations for the steady-state PEM fuel cell model consist of continuity, conservation of momentum and species transport. To represent the electrochemistry and transport phenomena through the membrane, appropriate source terms are applied at the anode and cathode catalyst layers.

The mass conservation equation (continuity equation):

$$\nabla (\rho\vec{u}) = 0 \qquad (1)$$

where ρ is the fluid density and $\vec{u}$ is the velocity vector.

The momentum conservation equation:

$$\nabla(\rho\vec{u}\vec{u}) = -\nabla P + \nabla(\mu\nabla\overrightarrow{u}) + S_u \qquad (2)$$

where P is the pressure and S_u is the source term.

In the porous region, Darcy's law term is added to the momentum equations to represent the momentum related with the resistance due to a porous media. The source term is expressed as:

$$S_u = -\frac{\mu \vec{u}}{K} \quad (3)$$

The species conservation equation:

$$\nabla(\rho \vec{u} \overrightarrow{X_k}) = \nabla(D_k^{eff} \rho \nabla \overrightarrow{X_k}) + S_k \quad (4)$$

where index *k* refers to different species, X_k is the molar concentration of species *k* and $D_k{}^{eff}$ is the effective diffusivity of species *k*. The diffusivity in the gas channel can be expressed as [6]:

$$D_k = D_{k,ref} \left(\frac{T}{T_{ref}}\right)^{3/2} \left(\frac{P_{ref}}{P}\right) \quad (5)$$

where $D_{k,ref}$ is the reference value at T_{ref} and P_{ref}.

The effective diffusivity of species can be described by the Bruggeman correction [6]:

$$D_k^{eff} = \epsilon^{1.5} D_k \quad (6)$$

The source terms (S_k) in the species conservation equation are defined as zero for all regions of the model except the catalyst layers. The species source term for the anode and cathode catalyst layers are expressed as:

Consumption of hydrogen due to electrochemical effects at the anode catalyst layer

$$S_{H_2} = -\frac{IA}{2F} M_{H_2} \quad (7)$$

Consumption of oxygen due to electrochemical effects at the cathode catalyst layer

$$S_{O_2} = -\frac{IA}{4F} M_{O_2} \quad (8)$$

Production of water and flux of water due to electrochemical effects at the cathode catalyst layer

$$S_{cw} = \frac{[1+2\alpha]IA}{2F} M_{H_2O} \quad (9)$$

Flux of water due to electrochemical effects at the anode catalyst layer

$$S_{aw} = -\frac{\alpha IA}{F} M_{H_2O} \quad (10)$$

The average current density *I* and net water transfer coefficient α are used to determine these source terms. A number of auxiliary equations are needed to be solved to model the electrochemical reactions and determine the local current density and net water transfer coefficient. The empirical equations are based on the assumption of using the Nafion 117 membrane, and taken from the work of Springer *et al.* [22].

2.3 Auxiliary Equations

The auxiliary model equations, needed to be solved to determine the net water transfer coefficient and cell voltage at average current density, are summarized below:

Net water transfer coefficient [6]

$$\alpha = n_d - \frac{FD_{H_2O}[C_{H_2O_c} - C_{H_2O_a}]}{It_m} \quad (11)$$

Where D_{H_2O} represents the water diffusion coefficient, and $C_{H_2O_a}$ and $C_{H_2O_c}$ represent the molar concentration of water at the anode and cathode side respectively, *I* is the average current density and t_m is the membrane thickness and *F* is the Faraday's constant.

The electro-osmotic drag coefficient describes the amount of water dragged by each proton across the membrane from the anode to the cathode side and is expressed as, [6]

$$n_d = 0.0049 + 2.02a_a - 4.53a_a^2 + 4.09a_a^3 \; ; \; a_a \leq 1$$

$$n_d = 1.59 + 0.159(a_a - 1); \qquad a_a > 1 \quad (12)$$

Water activity is defined as, [6]

$$a_k = \frac{X_{H_2O,k}P}{D_{H_2O,k}^{sat}} \quad (13)$$

where P is the cell pressure and $X_{H_2O.K}$ is the mole fraction of water on either the anode or cathode side.

Water vapour saturation pressure is given by [6],

$$P_{H_2O,K}^{sat} = [0.00644367 + 0.000213948(T-273) + 3.43293\times10^{-5}(T-273)^2 - 2.70381\times10^{-7}(T-273)^3 + 8.77696\times10^{-9}(T-273)^4 - 3.14035\times10^{-13}(T-273)^5 + 3.82148\times10^{-14}(T-273)^6]1.013\times10^5 \quad (14)$$

Water diffusion coefficient is expressed as [6],

$$D_{H_2O} = 5.5e^{-11}n_d \exp\left[2416\left(\frac{1}{303}-\frac{1}{T}\right)\right] \quad (15)$$

Water concentration on the anode and cathode side, [6]

$$C_{H_2O,K} = \frac{\rho_{m,dry}}{M_{m,dry}}\left(0.043 + 17.8a_k - 39.8a_k^2 + 36.0a_k^3\right);\ a_k \le 1$$

$$C_{H_2O,K} = \frac{\rho_{m,dry}}{M_{m,dry}}(14 + 1.4(a_k - 1));\ a_k > 1 \quad (16)$$

2.4 Polarization Characteristics

When electrical energy is drawn from the cell, the cell potential drops due to irreversible losses (activation, ohmic and concentration overpotential). The cell voltage can be expressed by the following equation [17]:

$$V_{cell} = E - \eta_{act} - \eta_{ohm} - \eta_{conc} \quad (17)$$

where E is the equilibrium thermodynamic potential which is calculated using the Nernst equation [17]:

$$E = 1.23 - 0.9 \times 10^{-3}(T - 298) + 2.3\frac{RT}{4F}\log(p_h^2 p_o) \quad (18)$$

η_{act} is the activation overpotential, η_{ohm} is the ohmic overpotential and η_{conc} is the concentration overpotential.

- Activation overpotential η_{act}:

The activation overpotential is a function of local current density, exchange current density and concentration of oxygen. The activation overpotential is expressed by the Butler-Volmer equation, [17]

$$i_a = i_{a,ref}\left(\frac{C_h}{C_{h,ref}}\right)^{\frac{1}{2}}\left\{exp\left[\frac{\alpha_a \eta_a F}{RT}\eta_{act,a}\right] - exp\left[-\frac{(1-\alpha_a)\eta_a F}{RT}\eta_{act,a}\right]\right\}$$

$$i_c = i_{c,ref}\left(\frac{C_o}{C_{o,ref}}\right)^{\frac{1}{2}}\left\{exp\left[\frac{\alpha_c \eta_c F}{RT}\eta_{act,c}\right] - exp\left[-\frac{(1-\alpha_c)\eta_c F}{RT}\eta_{act,c}\right]\right\} \quad (19)$$

Where $i_{a,ref}$ and $i_{c,ref}$ are the exchange current density multiplied by the specific area, n is the electron number of the reaction at the anode or cathode and α is the transfer coefficient [17].

- Ohmic overpotential (η_{ohm}):

The ohmic overpotential occurs due to the resistance to electron and ion transfer and can be expressed as:

$$\eta_{ohm} = \eta_{ohm}^{el} + \eta_{ohm}^{pro} = I\left(R^{el} + R^{pro}\right) \quad (20)$$

Where R^{el} is the resistance to electron transfer and R^{pro} is the resistance to proton transfer. In the present model, $R^{el} = 0.1\ \Omega\ \text{cm}^2$ is assumed. R^{pro} is calculated using the following expression:

$$R^{pro} = \frac{t_m}{k_m} \tag{21}$$

t_m is the height of the membrane and k_m is the phase conductivity of the membrane. The membrane phase conductivity depends on the temperature and water concentration at the anode side and is expressed as

$$k_m = 100\left[0.00514\left(\frac{M_{m,dry}}{\rho_{m,dry}}\right)C_{H_2O_a} - 0.00326\right]\exp\left[1268\left(\frac{1}{303} - \frac{1}{T}\right)\right] \tag{22}$$

- Concentration overpotential (η_{conc}):

At high current densities, polarization losses are dominated by the concentration overpotential which is caused by slow diffusion of the gas phase through the porous regions. The concentration overpotential can be determined by:

$$\eta_{conc} = -\frac{RT}{nF}\ln\left(1 - \frac{1}{I_L}\right) \tag{23}$$

where I_L is the limiting current density:

$$i_L = \frac{nFD_h C_{k,o}}{H_d} \quad (24)$$

2.5 Diffusion Models

The effective diffusivity through a porous medium can be expressed as

$$D_k^{eff} = f(\varepsilon) D_k \quad (25)$$

where D_k^{eff} is the effective diffusivity and D_k is diffusivity of the species in a plain medium. $f(\varepsilon)$ is a function of porosity and various correlations are available to determine this function. Most of the PEM fuel cell models use the Bruggeman correlation to explain the diffusion of species through porous gas diffusion layers and catalyst layers. Various other correlations have been considered in this paper.

According to the Bruggeman correlation, the function can be expressed as,

$$f(\varepsilon) = \varepsilon^{1.5} \quad (26)$$

Dawes *et al.* [13] developed a percolation theory based effective diffusivity model, where the function is expressed as,

$$f(\varepsilon) = \frac{(\varepsilon - 0.11)^{0.9}}{(1 - 0.11)^{0.9}} \quad (27)$$

Neale and Nader [23] used the following correlation to explain the diffusion through an isotropic porous medium;

$$f(\varepsilon) = \frac{2\varepsilon}{3-\varepsilon} \quad (28)$$

Mezedur et al. [11] suggested a diffusion model for a multi-length scale, particle based porous medium as

$$f(\varepsilon) = [1-(1-\varepsilon)^{0.46}] \quad (29)$$

Tomadakis and Sotirchos [10] suggested the following percolation theory based diffusion model for random fibrous porous medium

$$f(\varepsilon) = \varepsilon \left(\frac{\varepsilon-\varepsilon_p}{1-\varepsilon_p}\right)^{\alpha} \quad (30)$$

where ε_p is the percolation threshold and equal to 0.11. α is an empirical constant which depends on the direction. α is 0.521 and 0.785, for in-plane and through-plane diffusion, respectively.

Table 1

Physical parameters and boundary conditions used for the base case simulation

Gas channel length	L= 100 mm	
Gas channel width	W = 1 mm	[17]
Gas channel height	H_{ch} = 1 mm	[17]
Diffusion layer height	H_d = 0.254 mm	[16-17]
Catalyst layer height	H_{ct} = 0.0287 mm	[16-17]
Land area width	W_l = 1 mm	[17]
Membrane thickness	t_m = 0.23 mm	[24]
Permeability	K = 1.76x 10^{-11} m^2	[16-17]
Faraday Constant	F = 96485.309 C mol^{-1}	
Operating pressure	P = 101325 Pa	
Operating temperature	T = 323 K	[24]
GDL porosity	ε_{gdl} = 0.4	[16]
CL porosity	ε_{cl} = 0.4	
Dry mass of membrane	$M_{m,dry}$ = 1.1 $kgmol^{-1}$	
Dry density of membrane	$\rho_{m,dry}$ = 2000 kgm^{-3}	
Fuel/ air stoichiometric ratio	ξ_a/ξ_c= 5/5	[24]
Electron number of anode Reaction	n_a = 4	
Electron number of cathode Reaction	n_c = 2	
Relative humidity of inlet fuel	RH_a = 100%	[24]
Relative humidity of inlet air	RH_c = 0%	[24]
Oxygen mass fraction of inlet air	ω_O = 0.232	
H_2 diffusion coefficient at reference state	$D_{h,\,ref}$ = 0.915 × 10^{-4} m^2s^{-1}	[17]
Oxygen diffusion coefficient at reference state	$D_{O,\,ref}$ = 0.22 × 10^{-4} m^2s^{-1}	[17]
Water vapour diffusion coefficient at reference state	$D_{w,\,ref}$ = 0.256 × 10^{-4} m^2s^{-1}	[17]
Anode exchange current density	$i_{a,ref}$ = 2.0 × 10^8 Am^{-3}	[17]
cathode exchange current density	$i_{c,ref}$ = 160 Am^{-3}	[17]
Hydrogen reference concentration	$C_{h,ref}$ = 56.4 mol m^{-3}	[17]
Oxygen reference concentration	$C_{o,ref}$ = 3.39 mol m^{-3}	[17]
Anode transfer coefficient	α_a = 0.5	[17]
Cathode transfer coefficient	α_c= 0.5	[17]

2.6 Numerical procedure

The governing equations and the auxiliary equations have been solved to investigate the complex electrochemical processes and transport phenomena using a finite volume CFD method. The convection term in the governing equations have been descretised by second order upwind and the diffusion terms by the hybrid scheme. The SIMPLE algorithm has been selected at the pressure-velocity coupling. Appropriate source terms have been applied to the governing equations for the catalyst layers using user defined functions. The source terms, diffusivity model and electrochemistry algorithm were written in C++ UDFs which has been interpreted by the CFD solver FLUENT. An explicit electro-chemistry model has been used where an average current density has been specified and all other electro-chemical parameters have been calculated based on the iterative solution of the conservation equations of the mass fraction of species. Since the focus of the present study is on species transport, the explicit electrochemistry modelling allows reducing modelling complexity without the need for solving the transport equation for electric potential, but at the same time allows the investigation of diffusion of species through the GDL realistically. It would, however, be interesting to investigate the anisotropic electrical resistance through solving a transport equation of electric potential in future work. A symmetry boundary condition has been applied on the side surfaces of the porous regions (Fig. 1). No slip condition has been applied to the external walls. The solution of the governing conservation equations has been considered to be converged when the relative residual reached below 10^{-6}.

2.7 Computational domain and physical parameters

A representative section of a PEM fuel cell comprised of a three-dimensional straight channel has been considered in the present study (Fig. 1). The geometry is similar to the computational work of Liu [16] and Min [17]. Physical dimensions of the computational domain as well as relevant fuel cell parameters are given in Table 1. The computational domain has been meshed with quadrilateral grids of 12700 cells. A grid sensitivity test using up to 480000 cells has proved that the grid size of 12700 cells is sufficient to provide grid independency. Simulations have been carried out on a quad core Xeon workstation running on serial server. Each simulation took approximately 1000 iterations to converge in approximately 15 minutes of run time.

3 RESULTS AND DISCUSSION

3.1 Effects of effective diffusivity

The predominate flow direction within a parallel or serpentine fuel cell channel is longitudinal. However, in order for the reaction to take place, the reactants flow through the GDL to the catalyst layer. The flow of the reactants in the GDL is perpendicular to main the flow direction. It is therefore expected that the diffusion of species plays a key role in species transport and this is the focus of the present study. Figure 2 shows a comparison of various diffusivity models against the most widely used Bruggeman model. Dawes et al [13] and Neale and Nader [23] models produce higher values of effective diffusivity compared to the Bruggeman over the whole range of porosity, whereas the Mezedur et al [11] model starts at higher values, but quickly falls

below the Bruggeman model. Tomadakis and Sotirchos [10] is the only model that takes into account the anisotropy of the GDL layer and shows the in-plane permeability is greater than the through-plane permeability and that both the in-plane and through-plane permeability are lower than the Bruggeman model. The porosity of the GDL in the present model has been taken as 0.4. At this porosity, Dawes [13] model predicts 40% and Neale and Nader model [23] predicts 20% higher effective diffusivity compared to the Bruggeman model and Mezedur et al [11], Tomadakis and Sotirchos [10] in-plane and through-plane models predict 10%, 20% and 35% lower diffusivity compared to the Bruggeman model. Clearly each of these diffusivity models produces a widely different estimate and it is not entirely clear which of these models is a better fit for the numerical modeling of the gas diffusion layer of a PEM fuel cell. The reason behind the wide differences in the trend of the effective diffusivity seem to stem from the fact that these correlations were developed and fitted to certain experimental results and geometries and none of these experiments and models used similar geometry and physical parameter values. The reported correlations for the effective diffusivity were developed for different porous media, for example, packed spherical particles (Bruggeman and Neale and Nader model [23]), multi-length scale particles based porous media (Mezedur et al [11]), isotropic fibrous web (Dawes [13]) and anisotropic fibrous web (Tomadakis and Sotirchos [10]). The extent to which these differences in the effective diffusivity contribute to the overall fuel cell performances has been discussed below.

Figure 3 shows the effect of effective diffusivity on the fuel cell performance at different current densities. The figure also shows experimental data of Ticianelli et al [24]. For average current densities below 0.5 Acm^{-2}, smaller differences in cell voltages among different diffusivity models have been observed. While, for higher current densities significant variations have been

observed up to an average current density of 1 Acm^{-2}. Both Mezedur et al [11] and Tomadakis and Sotirchos [10] model provide a much closer prediction compared to the experimental data. In particular, Tomadakis and Sotirchos [10] model prediction is very close to experimental data, though there is still a discrepancy between the simulation and experimental value. This discrepancy can be attributed to the single phase modeling of water. The water has been considered to be present only in vapour form in the present study. The experimental data of Ticianelli et al [24] has been widely used as a kind of benchmark for validating numerical modeling [16, 25]. However, the exact geometry of the fuel cell used in the experiment of Ticianelli [24] is unknown. The operating pressure, temperature and the Nafion 117 membrane used in the Ticianelli et al experiment [24] have been utilised in the present study. Where relevant parameters are not known from the Ticianelli et al experiment [24], these have been taken from previous reported modeling studies [16-17, 25] and are given in Table 1. It should be noted that the ability of the present model to reproduce the experimental polarization curve is a necessary validation check, but is not particularly informative as any modelling study can reproduce the experimental data by adjusting some of the many parameters involved. The strength of the present modelling study lies in providing detailed insight into the transport mechanism and its interactions.

To understand the variation of cell performance with diffusivity models, oxygen and water vapour contour plots from the cathode side have been plotted. Figure 4 shows the oxygen contour plots of the catalyst/membrane interface at 0.5 Acm^{-2} and 1.0 Acm^{-2}. At both current densities, the mass fraction of oxygen has been overpredicted by Dawes et al [13] and Neale and Nader [23] models compared to the Bruggeman, while the Mezedur et al [11] and Tomadakis and Sotirchos [10] model underpredict the mass fraction of oxygen. This effect is more prominent at the higher

current density. A closer inspection of the mass fraction of oxygen predicted by Tomadakis and Sotirchos [10] model reveals a much more uniform oxygen distribution due to taking into account more realistic in-plane diffusion which is higher than the through-plane diffusion.

Figure 5 shows the mass fraction of water vapour distribution predicted by various effective diffusivity models on the catalyst/membrane interface for 0.5 Acm^{-2} and 1.0 Acm^{-2} respectively. The predicted mass fraction of water vapour is higher under the land area compared to the channel area. There are large differences on the predicted peak values of water vapour among the different diffusivity models specially at 1.0 Acm^{-2} current density. Dawes et al [13] and Neale and Nader [23] models produce lower peak water vapour values compared to the Bruggeman model, whereas Mezedur et al [11] and Tomadakis and Sotirchos [10] produces higher water vapour level.

Water management is a big challenge which needs to be tackled for improving the performance of a PEM fuel cell. There are several techniques available to meet this challenge including optimising operating parameters (gas flow rate, pressure, temperature, relative humidity, stoichiometry etc.) and flow field design and configurations [26-27]. In addition, extra systems and components (extra valves, electro-osmotic pumps, and acoustic wafers) have been shown to improve fuel cell performance by removing water quickly [26-27]. However, these extra components lead to increased complexity and parasitic losses. Therefore, there is a continued need for model development and parametric study for optimising operating conditions and flow field design for water management. The main implication of the present finding is that any water management strategy developed based on the Bruggeman correlation may lead to inadequate water removal from the GDL.

3.2 Effect of GDL permeability

In order to investigate the effects of GDL permeability on cell performance, simulations have been carried out for a range of permeability ($\mathbf{1 \times 10^{-10}}$ m^2 to $\mathbf{1 \times 10^{-14}}$ m^2). These values have been chosen as the most representative values of commonly used GDLs in the reported experimental and numerical studies. Table 2 shows the combinations of different case studies. C stands for case studies in the table. C11, C22 and C33 stand for isotropic permeability combinations. Similarly, C12, C13, C21, C23, C31 and C32 stand for anisotropic permeability combinations. Though various combinations of permeability values have been simulated, in practice, the in-plane permeability of GDL is much higher than the through-plane permeability. Therefore, cases C11, C12, C13 are of greater relevance to the practical situation and have been reported here. Simulations have been carried out to investigate the effect of permeability at average current densities of 0.5 and 1 Acm^{-2}. The catalyst layer permeability has been fixed for all the case studies at 1 x 10^{-10}.

Table 2

Combinations of permeability for the model study

In plane Permeability x-z direction	Through plane Permeability y direction		
	$1x10^{-10}$	$1x10^{-12}$	$1x10^{-14}$
$1x10^{-10}$	C11	C12	C13
$1x10^{-12}$	C21	C22	C23
$1x10^{-14}$	C31	C32	C33

Figure 6 shows vector plots at the mid plane of the assembly at different permeability cases (C11, C12, C13, C22, and C33). In these plots vector lengths are kept constant as the velocity varies widely among different zones. At the high permeability case, the velocity direction is mainly longitudinal inside the GDL (C11) caused by the high convective velocity in the flow channel. At low permeability cases however (C22 and C33) the direction of flow changes inside the GDL, and becomes perpendicular to the main flow directions. This is more evident in the anode as the velocity in the anode channel is much lower than in the cathode channel. In the case of anisotropic permeability (C12 and C13), the velocity vector plots are quite similar to C11 highlighting that the effects of lower through plane permeability is negligible.

The cell voltage predictions obtained from the simulations have been summarised in Table 3. It is observed from the Table 3, for the isotropic simulation cases (C11, C22, C23), that the effect of permeability is negligible at both current densities. Again for anisotropic permeability combinations from C11 to C13, the effect of anisotropy on cell voltage is negligible. The effects of permeability (both isotropic and anisotropic) are insignificant on both oxygen and water vapour distribution as shown in Figures 7 and 8. These figures show the profile of mass fraction of oxygen and water vapour at the GDL/CL interface at the inlet, middle and outlet locations. Dawes et al [13] have also shown that the effects of permeability on current density ceases below a permeability of 5×10^{-11}. It can be safely concluded that the uncertainty in the permeability value has less of an effect on the cell performance compared to the effective diffusivity as the dominant force for species transport through a GDL is diffusion. Ahmed et al [21] have also shown that the effects of anisotropy are negligible if the permeability is high in one direction.

Table 3

Cell Voltage at isotropic and anisotropic conditions

Case Studies	Cell Voltage	
	0.5 Acm-2	1.0 Acm-2
C11	0.596	0.237
C22	0.594	0.233
C33	0.594	0.232
C12	0.594	0.233
C13	0.594	0.233

4 CONCLUSION

Numerical Modelling plays a significant role in optimizing performance and developing new architectures for PEM fuel cells. Developing an accurate computational model involving a complex set of parameters is challenging. Moreover, there are many uncertainties in specifying different physical parameters. In this study, a three-dimensional, steady state, single phase, explicit electro-chemistry PEM fuel cell model has been developed to study the effects of two such parameters, the effective diffusivity and permeability of a gas diffusion layer.

The diffusion of species through a gas diffusion layer has been modeled by using the Bruggeman, Dawes et al [13], Neale and Nader [23], Mezedur et al [11], Tomadakis and Sotirchos [10]. Among these models, Tomadakis and Sotirchos [10] is the only model which takes into account the anisotropy of fibre distribution, whereas the Bruggeman correlation is the most widely used effective diffusivity model for PEM fuel cell Modelling. Simulation results show that the effective diffusivity model has significant effects on the prediction of fuel cell performance. Dawes, and Neale and Nader models provide higher values of cell voltage compared to the Bruggeman model, while Mezedur et al, Tomadakis and Sotirchos anisotropic

models produce lower values of voltage compared to the Bruggeman model. The Tomadakis and Sotirchos anisotropic model produces a cell voltage much closer to the experimental values.

The simulation result shows significant changes in the flow direction inside the GDL layer for lower isotropic permeability cases. For anisotropic permeability where the in-plane permeability is higher than through plane permeability, there appears to be small changes in the flow direction. In addition, the simulation results show that the effect is insignificant in cell voltage prediction for isotropic and anisotropic cases within the realistic permeability range of 10^{-10} to 10^{-14}.

The main conclusion from the study is that the effect of effective diffusivity is significant and the anisotropic diffusivity model should be utilized in PEM fuel cell Modelling. The effect of permeability is found to be insignificant and any realistic value of permeability could be safely specified in a PEM fuel cell Modelling.

NOMENCLATURE

a_k	water activity
A	specific area of the catalyst layer (m^{-1})
C	molar concentration (mol m^{-3})
D	diffusion coefficient (m^2 s^{-1})
E	equilibrium thermodynamic potential (V)
F	Faraday constant (96485.309 C mol^{-1})
H	Height (m)
i	reaction rate (Am^{-3})
I	average current density (Am^{-2})
K	permeability (m^2)
L	length (m)
M	molar mass (kg mol^{-1})
$M_{m,dry}$	dry mass of membrane (Kg mol^{-1})
n	electron number for reactions
n_d	electro-osmotic drag coefficient
P	pressure (Pa)

R	gas constant (8.314 J mol^{-1} K^{-1})
RH	relative humidity
S	source term
T	temperature (K)
$\boldsymbol{u}$	velocity vector (m s^{-1})
V_{cell}	cell voltage (V)
W	width (m)
X	molar fraction

Greek symbols

α	net water transfer coefficient
ε	porosity
η	overpotential (V)
μ	viscosity (kg m^{-1} s^{-1})
ρ	density (kg m^{-3})
ω	mass fraction
ζ	stoichiometric ratio

Subscripts and superscripts

0	before diffusion layer
a	anode
act	activation
av	average
c	cathode
conc	concentration
eff	effective
H_2	hydrogen
k	species
L	limiting
m	membrane
O_2	oxygen
ohm	ohmic polarization
ref	reference
w	water

ACKNOWLEDGMENTS

This project was funded by Northern Research Partnership (NRP) and IDEAS Research Institute, The Robert Gordon University, Aberdeen, UK.

REFERENCES

1 Energy White Paper: Meeting the Energy Challenge, 2006. http://www.dtistats.net/ewp/

2 World Wind Energy Association. http://www.wwindea.org/home/index.php?option=com_content&task=blogcategory&id=21&Itemid=43

3 Dutta, S., Shimpalee, S. and Van Zee, J. W. Numerical prediction of mass-exchange between cathode and anode channels in a PEM fuel cell. Int. J. Heat Mass Tran., 2001, 44 (11), 2029-2042.

4 Um, S. and Wang, C. Y. Three-dimensional analysis of transport and electrochemical reactions in polymer electrolyte fuel cells. J. Power Sources, 2004, 125(1), 40-51.

5 Nguyen, P. T., Berning, T. and Djilali, N. Computational model of a PEMFC with serpentine gas flow channels. J. Power Sources, 2004, 130,149-157.

6 Lum, W. K. and McGuirk, J. J. Three-dimensional model of a complete polymer electrolyte membrane fuel cell-model formulation, validation and parametric studies. J. Power Sources, 2005, 143 (1-2), 104-124.

7 Sivertsen, B. R. and Djilali, N. CFD-based modeling of proton-exchange membrane fuel cells. J. Power Sources, 2005, 141 (1), 65-78.

8 Pharoah, J. G., Karan, K. and Sun, W. On effective coefficients in PEM fuel cell electrodes: anisotropy of the porous transport layers. J. Power Sources, 2006, 161, 214-224.

9 Nam, J. H. and Kaviany, M. Effective diffusivity and water-saturation distribution in single- and two-layer PEMFC diffusion medium. Int. J. Heat Mass Tran., 2003, 46, 4595-4611.

10 Tomadakis, M. M. and Sotirchos, S. V. Ordinary and transition regime diffusion in random fiber structures. AIChE J., 1993, 39, 397-412.

11 Mezedur, M., Kaviany, M. and Moore, W. Effect of pore structure, randomness and size on effective mass diffusivity. AIChE J., 2002, 48, 15–24.

12 Gostick, J. T., Fowler, M. W., Pritzker, M. D., Ioannidis, M. A. and Behra, L. M. In-plane and through-plane gas permeability of carbon fiber electrode backing layers. J. Power Source, 2006, 162, 228-238.

13 Dawes, J. E., Hanspal, N. S., Famioly, O. A. and Turan, A. Three-dimensional CFD modeling of PEM fuel cells: an investigation into the effects of water flooding. Chem. Eng. Sci., 2008, 64, 2781-2794.

14 Bapat, C. J. and Thynell, S. T. Effect of anisotropic thermal conductivity of the GDL and current collector rib width on two-phase transport in a PEM fuel cell. J. Power Sources, 2008, 179, 240-251.

15 Ju, H. Investigation of the effects of the anisotropy of gas diffusion layers on heat and water transport in polymer electrolyte fuel cells. J. Power Sources, 2009, 191, 259-268.

16 Liu, X., Tao, W., Li, Z. and He, Y. Three-dimensional transport model of PEM fuel cell with straight flow channels. J. Power Sources, 2006, 158, 25-35.

17 Min, C. H. Performance of a proton exchange membrane fuel cell with stepped flow field design. J. Power Sources, 2009, 186, 370-376.

18 Wang, L., Husar, A., Zhou, T. and Liu, H. A parametric study of PEM fuel cell performances. Int. J. Hydrogen Energ., 2003, 28, 1263-1272.

19 Meng, H. Numerical investigation of transient responses of a PEM fuel cell using a two-phase non-isothermal mixed-domain model. J. Power Sources, 2007, 171, 738-746.

20 Simpalee, S. and Van Zee, J. W. Numerical studies on rib and channel dimension of flow-field on PEMFC performance. Int. J. Hydrogen Energ., 2007, 32, 842-856.

21 Ahmed, D. H., Sung, H. J. and Bae, J. Effect of GDL permeability on water and thermal management in PEMFCs – I. Isotropic and anisotropic permeability, Int. J. Hydrogen Energ., 2008, 33 , 3767-3785.

22 Springer, T. E., Zawodzinski, T. A. and Gottesfeld, S. Polymer electrolyte fuel cell model, J. Electrochem. Soc., 1991, 138 (8), 2334–2342.

23 Neale, G. H. and Nader, W. K. Prediction of transport processes within porous media - diffusive flow processes within a homogeneous swarm of spherical-particles, AIChE J. 1973, 19, 112–119.

24 Ticianelli, E. A., Derouin, C. R. and Srinivasan, S. Localization of platinum in low catalyst loading electrodes to attain high power densities in SPE fuel cells. J. Electroanal. Chem., 1998, 251, 275-295.

25 Berning, T. Lu, D. M. and Djilali, N. Three-dimensional computational analysis of transport phenomena in a PEM fuel cell. J. Power Sources, 2002, 106, 284-294.

26 Anderson, R., Zhang, L., Ding, Y., Blanco, M., Bi, X. and Wilkinson, D.P. A critical review of two-phase flow in gas channels of proton exchange membrane fuel cells. J. Power Sources, 2010, 195, 4531-4553.

27 Li, H., Tang, Y., Wang, Z., Shi, Z., Wu, S., Song, D., Zhang, J., Fatih, K., Zhang, J., Wang, H., Liu, Z., Abouatallah, R., Mazza, A. A review of water flooding issues in proton exchange membrane fuel cell. J. Power Sources, 2008, 178, 103-117.

Figure 1: Schematic diagram of the three-dimensional PEM fuel cell model

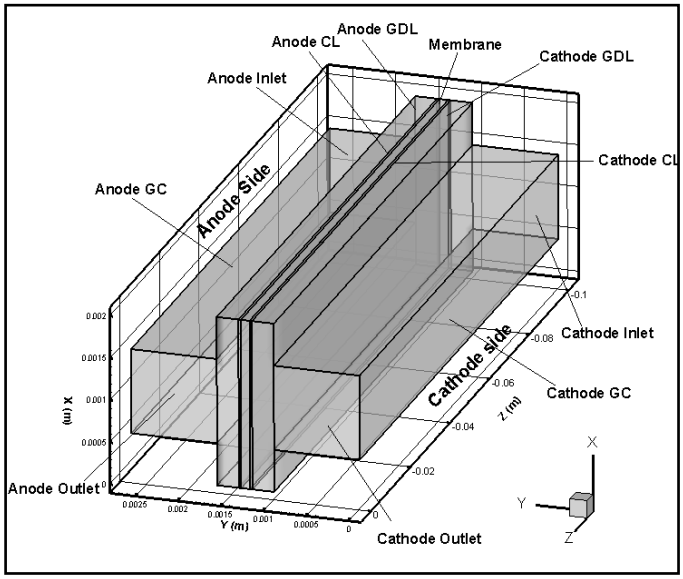

Figure 2: Comparison of effective diffusivity models at different porosity

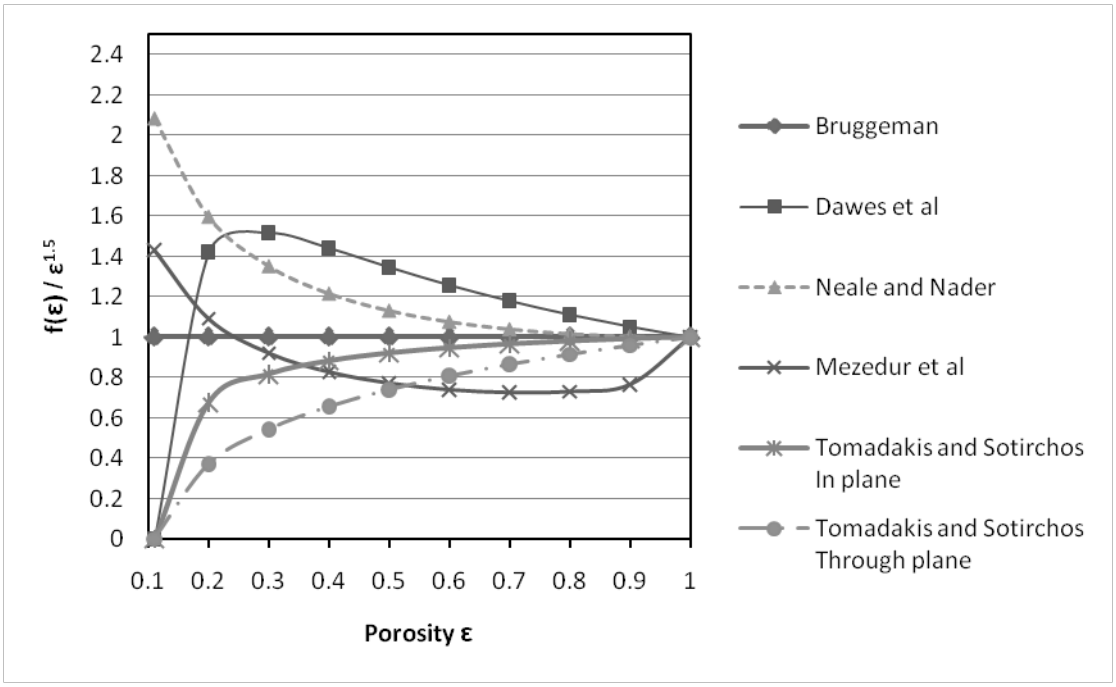

Figure 3: Comparison of diffusivity models for simulating voltage-current polarization curve

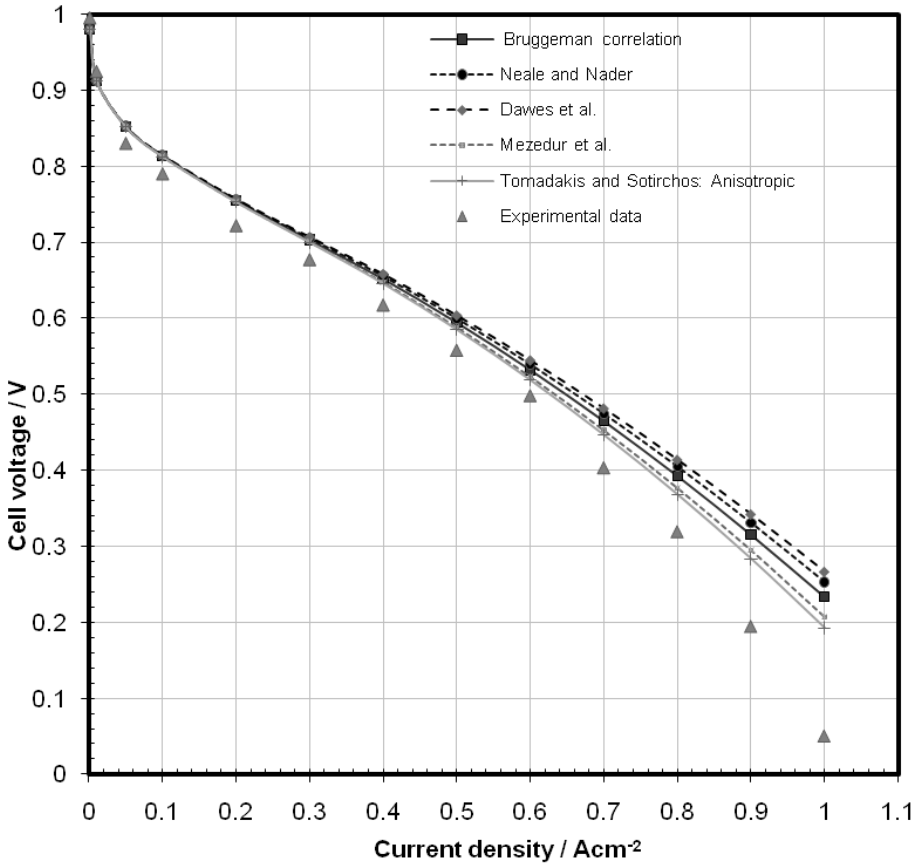

Figure 4: Contour of the mass fraction of oxygen at the catalyst/membrane interface

Figure 4

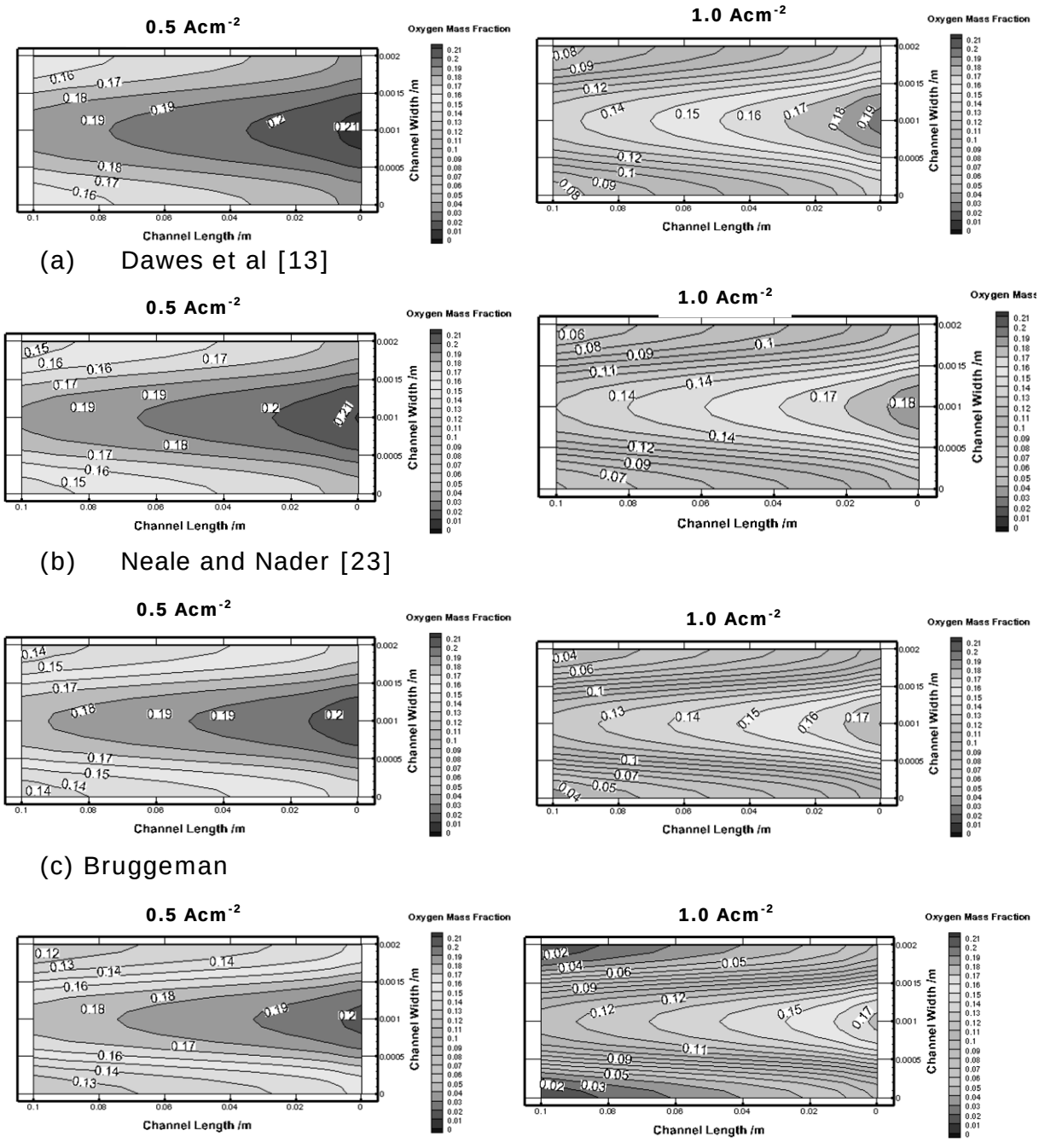

(a) Dawes et al [13]

(b) Neale and Nader [23]

(c) Bruggeman

(d) Mezedur et al [11]

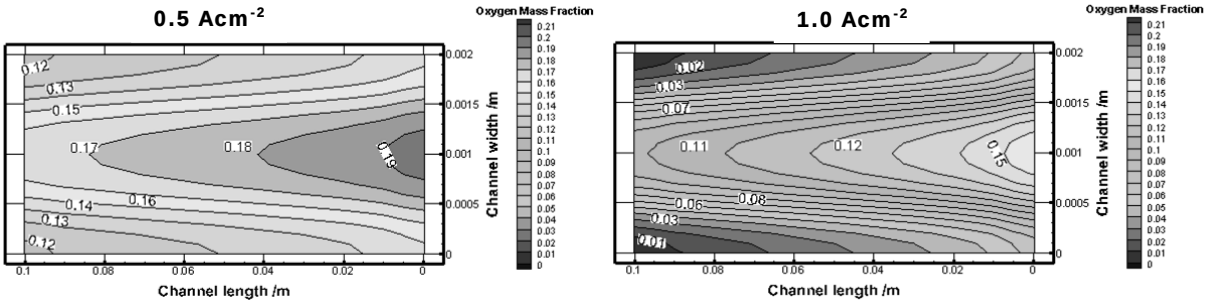

(e) Tomakadis and Sotirchos [10]

Figure 5: Contour of the mass fraction of water vapour at the catalyst/membrane interface

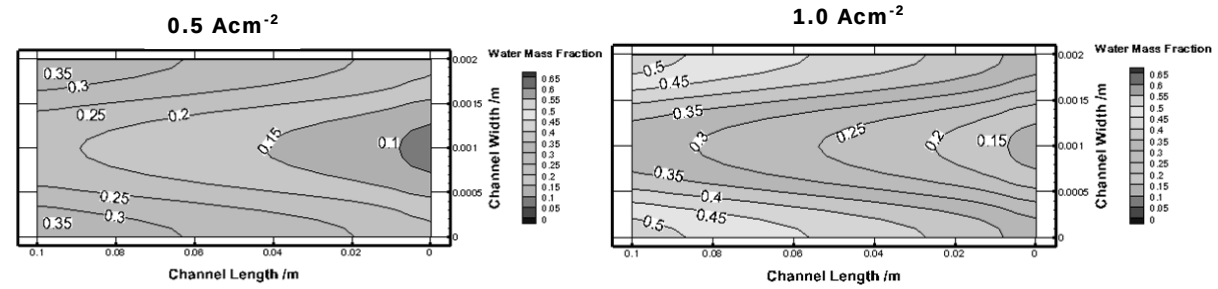

(a) Dawes et al [13]

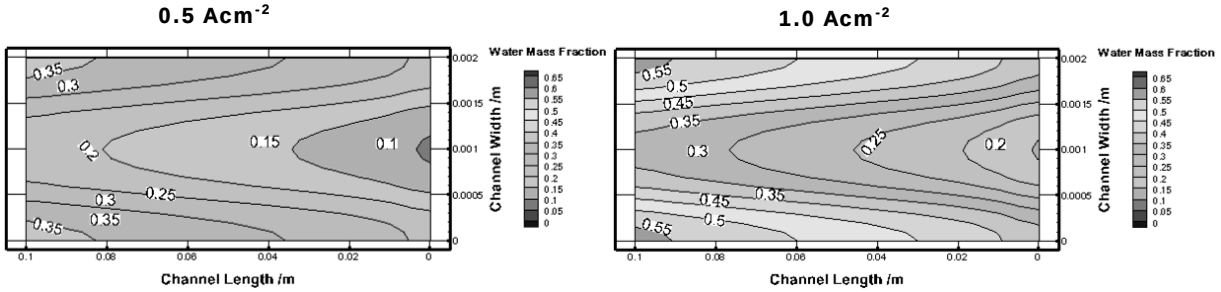

(b) Neale and Nader [23]

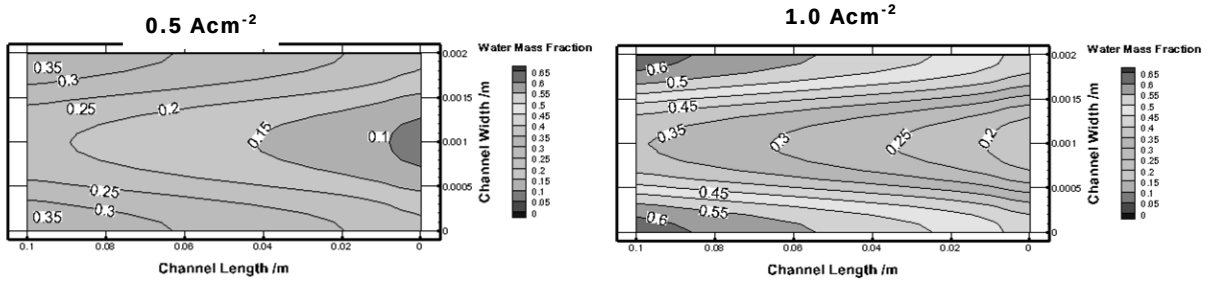

(c) Brugemman

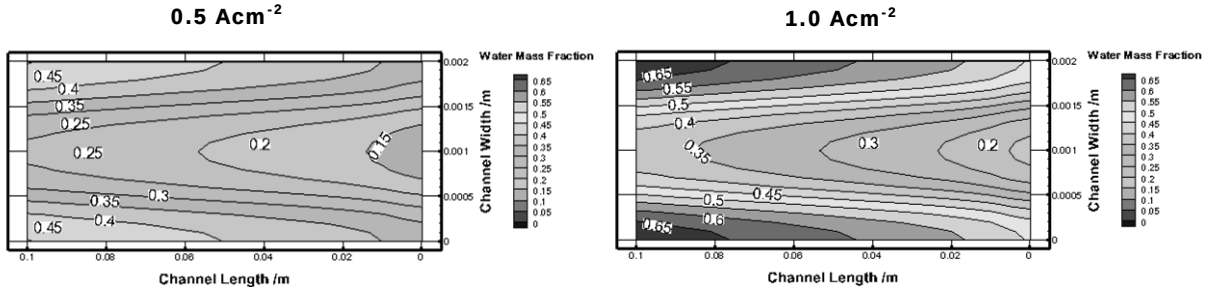

(d) Mezedur et al [11]

0.5 Acm^{-2} **1.0 Acm^{-2}**

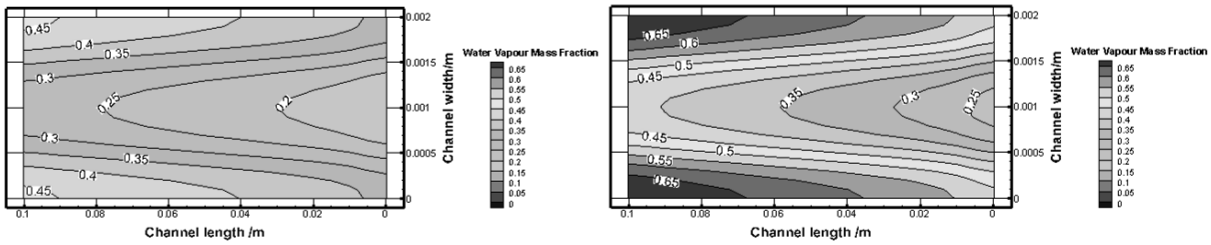

(e) Tomadakis and Storichos [10]

Figure 6: Velocity vector at midplane for different permeability cases

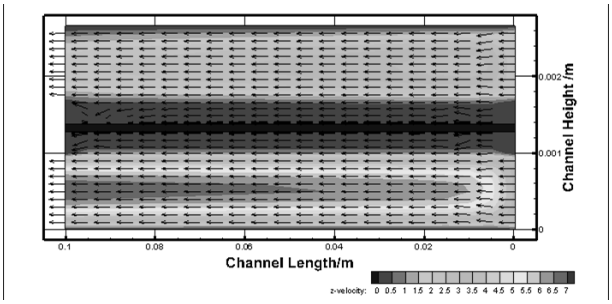

(a) C11

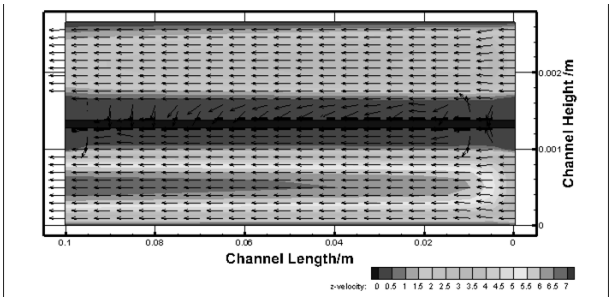

(b) C22

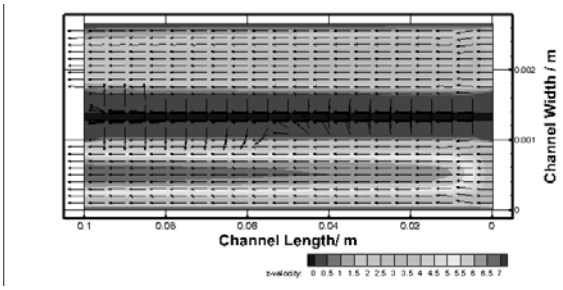

(c) C33

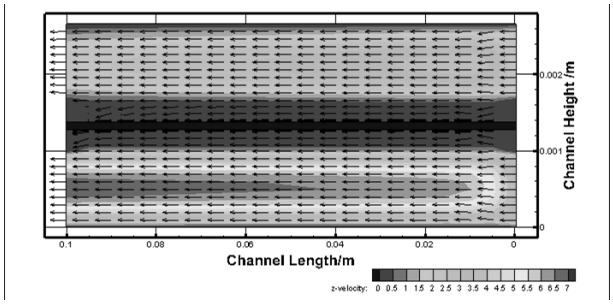

(d) C12

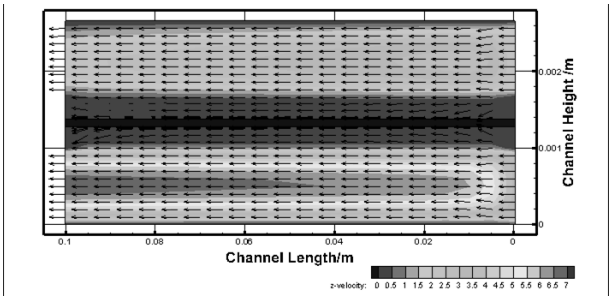
Channel Height /m
0.002
0.001
0
0.1
0.08
0.06
0.04
0.02
0
Channel Length/m
z-velocity: 0 0.5 1 1.5 2 2.5 3 3.5 4 4.5 5 5.5 6 6.5 7

(e) C13

Figure 7: Profile of the mass fraction of oxygen at the GDL/catalyst interface

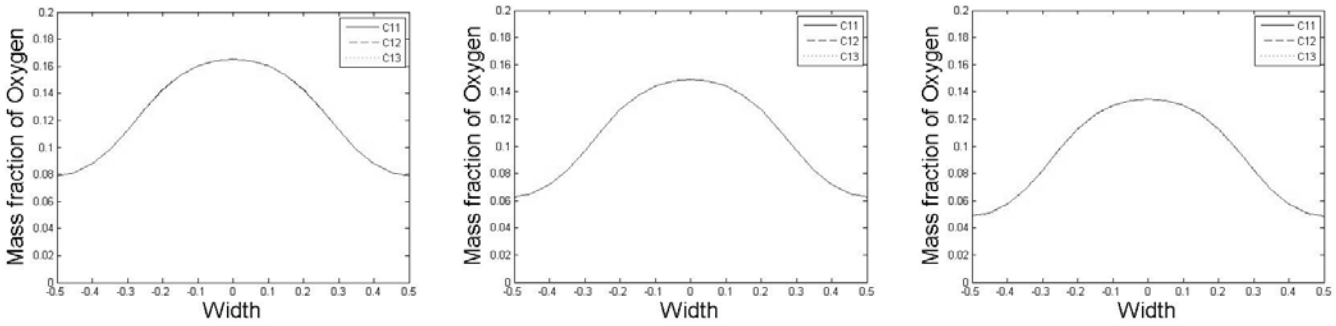

(a) inlet (b) middle (c) outlet

Figure 8: Profile of the mass fraction of water vapour at the GDL/catalyst interface

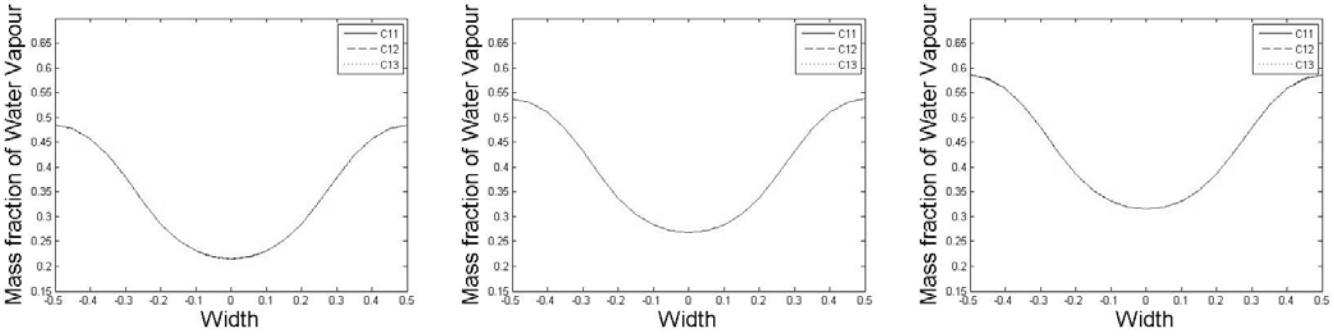

(a) inlet (b) middle (c) outlet